symmetry

MDPI

*Article*

# Entropy Generation for MHD Peristaltic Transport of Non-Newtonian Fluid in a Horizontal Symmetric Divergent Channel

**Kinda Abuasbeh [1,*], Bilal Ahmed [2,*], Azmat Ullah Khan Niazi [2] and Muath Awadalla [1]**

[1] Department of Mathematics and Statistics, College of Science, King Faisal University, Hofuf 31982, Al Ahsa, Saudi Arabia
[2] Department of Mathematics and Statistics, The University of Lahore, Sargodha 40100, Pakistan
* Correspondence: kabuasbeh@kfu.edu.sa (K.A.); bilalmaths7@yahoo.com (B.A.)

**Abstract:** The analysis in view is proposed to investigate the impacts of entropy in the peristaltically flown Ree–Eyring fluid under the stress of a normally imposed uniform magnetic field in a non-uniform symmetric channel of varying thickness. The administering equations of the present flow problem are switched into the non-dimensional form and then reduced by the availing of long wavelengths and creeping flow regime restrictions. The analytical treatment for the developed problem is performed to attain closed-form solutions which are further displayed as graphs of velocity, pressure, temperature, and entropy distribution. The trapping phenomenon has also been an area of our current examination. The role of relevant pronounced parameters such as the Brinkmann number, Hartmann number, and Ree–Eyring parameter for throwing vivid impacts are also concerned. It has been inferred that both the Brinkmann number and Ree–Eyring parameter with rising values inflate temperature and entropy profiles. The velocity profile shows the symmetric nature due to the horizontally assumed symmetric channel of varying thickness. The circulation of streamlines and bolus formations is visibly reduced in response to the increasing Hartmann number.

**Keywords:** peristaltic flow; Ree–Eyring fluid; entropy generation; magnetic field

check for updates

**Citation:** Abuasbeh, K.; Ahmed, B.; Niazi, A.U.K.; Awadalla, M. Entropy Generation for MHD Peristaltic Transport of Non-Newtonian Fluid in a Horizontal Symmetric Divergent Channel. *Symmetry* **2023**, *15*, 359. https://doi.org/10.3390/sym15020359

Academic Editors: Zivorad Tomovski and Jan Korbel

Received: 8 January 2023
Revised: 19 January 2023
Accepted: 24 January 2023
Published: 29 January 2023



## 1. Introduction

Generally, non-Newtonian fluids have acquired vast acceptance compared to Newtonian fluids due to an interdisciplinary approach, such as in chemical and allied processing industries and biomedical and physiological techniques. Pharmaceutical products, paints, varnishes, and waxy crude oils are a few distinctive forms that fall into the non-Newtonian category. The study of these fluids and their associated rheology are accomplished by numerous researchers and mathematicians to exploit their full potential in omnifarious geometries and physical conditions. Johnson [1] established the characterization and rheological aspects of elastohydrodynamic lubricants. Nouri et al. [2] explored Newtonian and non-Newtonian flows in fully developed annuli. A thorough and detailed inspection of rheology and non-Newtonian flows in various regimes was devised by Chhabra and Richardson [3]. Together with this, plenty of studies can be found in the literature [4–6] that uncover the characteristics connected with these fluids.

The wavelength motion of physiological fluids regulated by the compression of surrounding boundaries can be reflected through food swallowing in the esophagus, lymphocytes transmissions governed by the lymphatic system, blood flow in the vessels, urine passage to the bladder, and many other widespread precedents which have carved out the concept of peristalsis. On an industrial scale, roller and finger pumps, blood filtration equipment, and cardiopulmonary machines obey the principle of peristalsis. In the vibrating structure, the strain field changes the internal energy, and consequently, building the compressed sections of the high temperature can be conducted by considering the non-negative coefficient of thermal expansion and the expanded sections at low temperatures. The process responsible for thermoelastic damping is basically the loss of thermal equilibrium between various parts of the vibrating structure. The dissipated energy in an irreversible heat flow caused by the temperature gradient occurs.

The pioneer attempt in this regard was given by Latham [7]. Akram and Nadeem [8–10] examined the peristaltic motion of the Williamson fluid in an asymmetric conduit through an analytical approach and by observing distinctive peristaltic wave patterns. They also carried out an inspection for the peristaltically governed six constant Jeffrey's model in a two-dimensional channel. Pandey and Tripathi [11] modeled certain foodstuffs, such as the Casson model, to explore esophageal peristalsis in a finite channel. Mechanical efficiency concerned with the pumping and reflux mechanism was also taken into consideration. Ellahi et al. [12] considered the influence of bioheat transfer in a tapered rectangular duct with peristaltic consideration. Riaz et al. [13], by assuming the peristaltic progression of Jeffrey's model in a three-dimensional channel, extracted an exact solution by engaging slip limitations. They noted that the effects of slip limitations induced hindrance in the way of the flow. Further investigations were revealed for hyperbolic tangent fluid, six constant Casson fluids, and Eyring–Powell nanofluid in Refs. [14–16] in diverse geometries with several embedded effects.

The exposure of the magnetic field to the electrically conducting fluids makes the flow polarized and inversely distorts itself. The applications of the magnetic field in modern science and engineering are staggeringly endless. An analysis of the peristaltically navigated biofluid in an axisymmetric analog stressing under a magnetic field with altered viscosity was dealt with by the Adomian decomposition method (ADM) in [17]. Akbar [18] discussed peristaltically forcing the hydromagnetic Casson fluid in an asymmetric channel. Sinha et al. [19] proposed a theoretical analysis to uncover variable viscosity and the thermal and velocity impacts on peristaltic transport in an asymmetric channel. Bhatti et al. [20] divulged the peristaltic flow of Jeffrey fluid in a duct with wall properties which were influenced by a fluctuating magnetic field. By effectuating the perturbation approach, Abbas et al. [21] analyzed a drug delivery mechanism in the flow of blood induced by peristalsis-carrying nanoparticles. Abd-Alla [22] scrutinized the peristaltic conveyance of Jeffrey nanofluid in an inclined channel in addition to heat and mass transfer impacts which prompted an examination of concentration and temperature.

The system's disorder which has been stated as an irreversible process in which the heat energy generated is incapable of performing any useful work is usually called entropy. Several factors, such as viscous dissipation, abrupt thermal radiation, and Joule heating, are thought to create this uncertainty. It was Bejan [23] who first identified entropy generation in his heat conversion analysis. Akbar [24] showed that entropy profiles become escalated around the plumb duct while examining the peristaltic scheme for a carbon nanotube (CNT) suspension nanofluid. By ejecting inertial effects, Rashidi et al. [25] presented the analysis for entropy in peristaltically-induced blood flow with Lorentz force. By taking blood to be a magneto-micropolar fluid, the investigation carried out by Asha and Deepa [26] took the peristaltic flow in a non-uniform channel and talked about the impacts offered by entropy and heat radiation. Bibi and Hang Xu [27] elucidated the modeling of the peristaltic Jeffrey nanofluid flow influenced under a magnetic field in a symmetric channel. They illustrated entropy controlled by several estimations of pertinent parameters.

In non-Newtonian models, power law or the Ostwald de Waele model is likewise very functional in process engineering applications, but due to certain shortcomings, the Ree–Eyring model better fits to describe shear thinning and thickening effects. Its constitutive equations can be retrieved from the kinetic theory of fluids as opposed to an empirical relation. This kind of model has induced many studies which are available in the literature. Bhatti et al. [28] presented the study to analyze the role of the magnetic field and partial slip conditions on the peristaltic flow of the Ree–Eyring fluid and concluded that the velocity of the fluid is affected by the slip effects and effects of the magnetic field in a reverse attitude. Hayat et al. [29] provided the heat transfer analysis of the flow of the Ree–Eyring fluid in the rotation frame and deduced that the rotation parameter significantly influences the axial and secondary velocities, the size of the trapped bolus, and pressure rise per wavelength. The flow of the Ree–Eyring fluid in a duct in the presence of a magnetic field was considered by Ijaz et al. [30], who compared the behavior of the Newtonian with Ree–Eyring fluid. Hayat et al. [31] introduced the phenomenon of the homogeneous and heterogeneous reaction in the flow of the Ree–Eyring fluid and noticed that this affects the concentration alternatively. Tanveer and Muhammad [32] studied the peristaltic flow of the Ree–Eyring fluid in the slip and porosity in the presence of a magnetic field. Rajasekhar et al. [33] utilized the long wavelength and small Reynolds number to formulate the heat and mass transport impact on the peristaltic flow of Ree–Eyring fluid. Recently, Balachandran et al. [34] presented an analysis of peristaltic flow on the Ree–Eyring fluid in an inclined channel with variable fluid properties.

By keeping the notion of these examinations in our mind, the core objective of the current study is to expose thermal transfer and entropy generation in the passage of a non-Newtonian blood flow modeled with the Ree–Eyring fluid in a non-uniform symmetric channel and externally influenced by an orthogonally acting magnetic field. The differential equations indicating the physical principles are first transformed to their simplest form employing long wavelength and trivial Reynolds number. Subsequently, the solutions are gleaned analytically by exact methodology. In the later part, an ample discussion of the graphical outcomes is recorded by taking physical parameters into consideration.

## 2. Problem Formulation

The two-dimensional, viscous, unsteady, incompressible, non-Newtonian Ree–Eyring fluid is allowed to propel in a symmetric tapered channel. The source responsible for the flow generation is the peristaltic occurrence which is promoted by the spontaneous wave formation on the channel boundaries. The sketch of the under-considered problem is evident in Figure 1. The induction of regular oscillations along the walls led by the sinusoidal waves with a uniform speed $\widetilde{c}$ is described in the following fashion [35].

$$H(\widetilde{x},\widetilde{t}) = b(\widetilde{x}) + \widetilde{a}\sin\frac{2\pi}{\lambda}(\widetilde{x} - \widetilde{c}\widetilde{t}), \tag{1}$$

provided that $b(\widetilde{x}) = b_o + K_o\widetilde{x}$.

Where $b_o$ is the semi-width at the inlet of the non-uniform channel. $(K_o \ll 1)$ is constant. The semi-width $b$ as a function of axial distance $\widetilde{x}$ can be found at any location from the inlet. $\widetilde{a}$ and $\lambda$ define the amplitude and wavelength of the peristaltic waves, respectively. The problem has been dealt with in the rectangular coordinate system $(\widetilde{x}, \widetilde{y})$ in which velocities $\widetilde{u}$ and $\widetilde{v}$, respectively, are specified to be proportional to the axial coordinate $\widetilde{x}$ and transverse coordinate $\widetilde{y}$, whereas $\widetilde{t}$ is the time.

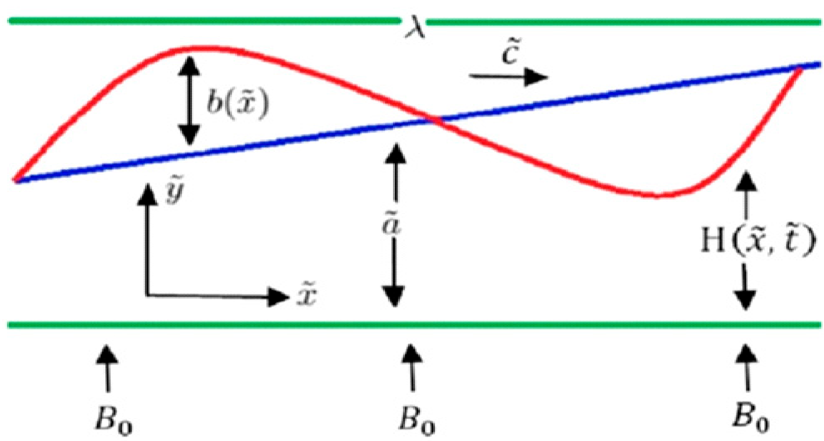


**Figure 1.** Schematic flow diagram for peristaltic transport of Ree–Eyring fluid.

The magnetic field of constant strength $B_o$ has also been observed in a direction normal to the flow, and due to the assumption of negligible electrical currents in comparison with the magnetic field, the induced magnetic field has been skipped.

The leading equations of continuity, momentum, and energy for the peristaltic drive of the Ree–Eyring model are described as [25]:

$$\frac{\partial \widetilde{u}}{\partial \widetilde{x}}+\frac{\partial \widetilde{v}}{\partial \widetilde{y}}=0, \tag{2}$$

$$\widetilde{\rho}\left[\frac{\partial \widetilde{u}}{\partial \widetilde{t}}+\widetilde{u}\frac{\partial \widetilde{u}}{\partial \widetilde{x}}+\widetilde{v}\frac{\partial \widetilde{u}}{\partial \widetilde{y}}\right]+\frac{\partial \widetilde{p}}{\partial \widetilde{x}}=\frac{\partial}{\partial \widetilde{x}}\tau_{\widetilde{x}\widetilde{x}}+\frac{\partial}{\partial \widetilde{y}}\tau_{\widetilde{x}\widetilde{y}}-\sigma B_o^2\widetilde{u}, \tag{3}$$

$$\widetilde{\rho}\left[\frac{\partial \widetilde{v}}{\partial \widetilde{t}}+\widetilde{u}\frac{\partial \widetilde{v}}{\partial \widetilde{x}}+\widetilde{v}\frac{\partial \widetilde{v}}{\partial \widetilde{y}}\right]+\frac{\partial \widetilde{p}}{\partial \widetilde{y}}=\frac{\partial}{\partial \widetilde{x}}\tau_{\widetilde{y}\widetilde{x}}+\frac{\partial}{\partial \widetilde{y}}\tau_{\widetilde{y}\widetilde{y}}-\sigma B_o^2\widetilde{v}, \tag{4}$$

$$\zeta_o\left[\frac{\partial T}{\partial \widetilde{t}}+\widetilde{u}\frac{\partial T}{\partial \widetilde{x}}+\widetilde{v}\frac{\partial T}{\partial \widetilde{y}}\right]=\frac{\kappa}{\widetilde{\rho}}\left(\frac{\partial^2 T}{\partial \widetilde{x}^2}+\frac{\partial^2 T}{\partial \widetilde{y}^2}\right)+\frac{\tau_{\widetilde{x}\widetilde{y}}}{\widetilde{\rho}}\left(\frac{\partial \widetilde{u}}{\partial \widetilde{y}}\right). \tag{5}$$

The renowned stress tensor of the Ree–Eyring fluid model can be written as [29]:

$$\boldsymbol{\tau}_{ij}=\mu\frac{\partial \widetilde{V}_i}{\partial \widetilde{x}_j}+\frac{1}{\overline{B}}\sin\mathrm{h}^{-1}\left(\frac{1}{\overline{C}}\frac{\partial \widetilde{V}_i}{\partial \widetilde{x}_j}\right), \tag{6}$$

As $\sin\mathrm{h}^{-1}\widetilde{x}=\widetilde{x}$ for $|\widetilde{x}|\leq 1$ holds, the above equation can be reduced more precisely to:

$$\boldsymbol{\tau}_{ij}=\mu\frac{\partial \widetilde{V}_i}{\partial \widetilde{x}_j}+\frac{1}{\overline{B}}\left(\frac{1}{\overline{C}}\frac{\partial \widetilde{V}_i}{\partial \widetilde{x}_j}\right), \tag{7}$$

where $\mu$ is the typical viscosity of the fluid and $\overline{B}$, $\overline{C}$ are, respectively, the material constants. Additionally, $\widetilde{\rho}$, $\widetilde{p}$, $\sigma$, $T$, and $\kappa$ designate the fluid's density, pressure, electrical conductivity, temperature, and the fluid's thermal conductivity.

The following dimensionless quantities are incorporated in order to obtain an improved version of the equations [29].

$$\left.\begin{array}{c} x=\frac{\widetilde{x}}{\lambda}, y=\frac{\widetilde{y}}{b_o}, u=\frac{\widetilde{u}}{\widetilde{c}}, v=\frac{\widetilde{v}}{\delta\widetilde{c}}, t=\frac{\widetilde{c}\widetilde{t}}{\lambda}, \delta=\frac{b_o}{\lambda}, h=\frac{H}{b_o}, p=\frac{b_o^2\widetilde{p}}{\lambda\mu\widetilde{c}}, \phi=\frac{\widetilde{a}}{b_o}, Re=\frac{\widetilde{\rho}\widetilde{c}b_o}{\mu}, \\ M=\sqrt{\frac{B_0^2 b_o^2\sigma}{\mu}}, \theta=\frac{T-T_o}{T_1-T_o}, Pr=\frac{\nu\zeta_o\widetilde{\rho}}{\kappa}, Ec=\frac{\widetilde{c}^2}{\zeta_o(T_1-T_o)}, B_r=PrEc, \zeta=\frac{1}{\mu BC} \end{array}\right\}, \tag{8}$$

where $\delta$, $\phi$, $\theta$, $Re$, $M$, $Pr$, $Ec$, $B_r$ and $\zeta$ are accounted for the wave number, amplitude ratio, non-dimensional temperature, Reynolds number, Hartmann number, Prandtl number, Eckert number, Brinkmann number, and Ree–Eyring fluid parameter, respectively. By substituting (8) in Equations (2)–(7), the following dimensionless form can be executed.

$$Re\delta\left(\frac{\partial u}{\partial t}+u\frac{\partial u}{\partial x}+v\frac{\partial u}{\partial y}\right)+\frac{\partial p}{\partial x}=(1+\zeta)\left(\delta^2\frac{\partial^2 u}{\partial x^2}+\frac{\partial^2 u}{\partial y^2}\right)-M^2u, \tag{9}$$

$$Re\delta^3\left(\frac{\partial v}{\partial t}+u\frac{\partial v}{\partial x}+v\frac{\partial v}{\partial y}\right)+\frac{\partial p}{\partial y}=\delta^2(1+\zeta)\left(\delta^2\frac{\partial^2 v}{\partial x^2}+\frac{\partial^2 v}{\partial y^2}\right)-\delta^2M^2v, \tag{10}$$

$$RePr\delta\left(\frac{\partial \theta}{\partial t}+u\frac{\partial \theta}{\partial x}+v\frac{\partial \theta}{\partial y}\right)=\left(\delta^2\frac{\partial^2 \theta}{\partial x^2}+\frac{\partial^2 \theta}{\partial y^2}\right)+PrEc(1+\zeta)\left(\frac{\partial u}{\partial y}\right)^2. \tag{11}$$

The implications of the long wavelength and insignificant Reynolds number suggest $\delta\to 0$ & $Re\to 0$. Then, the above equations take the given concise form.

$$\frac{\partial p}{\partial x}=(1+\zeta)\frac{\partial^2 u}{\partial y^2}-M^2u, \tag{12}$$

$$\frac{\partial p}{\partial y}=0, \tag{13}$$

$$\frac{\partial^2\theta}{\partial y^2}=-B_r(1+\zeta)\left(\frac{\partial u}{\partial y}\right)^2, \tag{14}$$

and the mandatory boundary conditions for above stated equations are mentioned as:

$$\frac{\partial u}{\partial y}=0,\ \theta=0 \text{ at } y=0, \tag{15}$$

$$u=0,\ \theta=1 \text{ at } y=h, \tag{16}$$

with the deformation in the wall in the dimensionless form of:

$$h=1+\frac{\lambda K_o x}{b_0}+\phi\sin 2\pi(x-t). \tag{17}$$

Equation (15) represents that there is no gradient of velocity and temperature at the center of the channel, while Equation (16) reflects that the heat is transferred from the walls of the channel, and the velocity of the fluid is zero at the wall.

## 3. Entropy Generation Analysis

The expression for volumetric entropy generation can be stated as:

$$s'''_{Gen}=\frac{\kappa}{T_o^2}\left(\frac{\partial T}{\partial\tilde{y}}\right)^2+\frac{1}{T_o}\left(\mu\tau_{\tilde{x}\tilde{y}}\left(\frac{\partial\tilde{u}}{\partial\tilde{y}}\right)+\sigma B_o^2\tilde{u}^2\right), \tag{18}$$

The three terms of entropy generation on the right-hand side of the above equation are due to thermal transfer irreversibility, viscous dissipation, and magnetic field.

In its dimensionless form, (18) can be related to the ratio of volumetric entropy generation $s'''_{Gen}$ to the characteristic entropy generation $s'''_G$.

$$N_s=\frac{s'''_{Gen}}{s'''_G}=\left(\frac{\partial\theta}{\partial y}\right)^2+\Lambda B_r(1+\zeta)\left(\frac{\partial u}{\partial y}\right)^2+\Lambda B_r M^2u^2, \tag{19}$$

where:

$$s'''_G=\kappa\left(\frac{T_1-T_o}{B_o^2T_o^2}\right),\ B_r=\frac{\tilde{c}^2\mu T_o}{\kappa(T_1-T_o)},\ \Lambda=\frac{T_o}{(T_1-T_o)}. \tag{20}$$

where $\Lambda$ is the temperature difference parameter.

## 4. Solution of the Problem

To acquire our solution, Equations (12) and (14) are subjected to integration twice so that we have:

$$u[y]=\frac{\frac{dp}{dx}\left[-1+\mathrm{Cosh}\left(\frac{My}{\sqrt{1+\zeta}}\right)\mathrm{Sech}\left(\frac{hM}{\sqrt{1+\zeta}}\right)\right]}{M^2}, \tag{21}$$

$$\theta[y]=\frac{1}{8hM^4}\left[\begin{array}{c}4M^4y-B_rP\frac{dp}{dx}^2(h-y)\left(-1+2hM^2y-\zeta\right)\\ +y\left(4M^4+B_r\frac{dp}{dx}^2(1+\zeta)\right)\mathrm{Cosh}\left(\frac{2hM}{\sqrt{1+\zeta}}\right)\\ -B_rh\frac{dp}{dx}^2(1+\zeta)\mathrm{Cosh}\left(\frac{2My}{\sqrt{1+\zeta}}\right)\left\{\mathrm{Sech}\left(\frac{hM}{\sqrt{1+\zeta}}\right)^2\right\}\end{array}\right], \tag{22}$$

where the instantaneous mean flow rate is represented as below that through which pressure gradient term can be extracted.

$$Q=-\frac{hM\frac{dp}{dx}+\frac{dp}{dx}\sqrt{1+\zeta}\,\mathrm{Tanh}\left(\frac{hM}{\sqrt{1+\zeta}}\right)}{M^3}, \tag{23}$$

$$\frac{dp}{dx} = -\frac{M^3 Q}{hM - \sqrt{1+\zeta}\,\mathrm{Tanh}\left(\frac{hM}{\sqrt{1+\zeta}}\right)} \tag{24}$$

The main advantage of the technique used in this study is that it gives an exact close-form solution to the problem considered and provides the most accurate results.

## 5. Results and Discussion

This section was established to look upon the vital role of influencing parameters to visualize the velocity, pressure, temperature, and entropy distribution in our evaluated results developed by utilizing Mathematica and MATLAB.

### *Validation*

The results obtained through the present considered model in special cases are validated against the results of Bhatti et al. [35]. The comparison of the pressure rise per wavelength is based on the present solution with the results of Bhatti et al. [35] and is plotted against the flow rate in the fixed frame in Figure 2, which was found in good agreement.

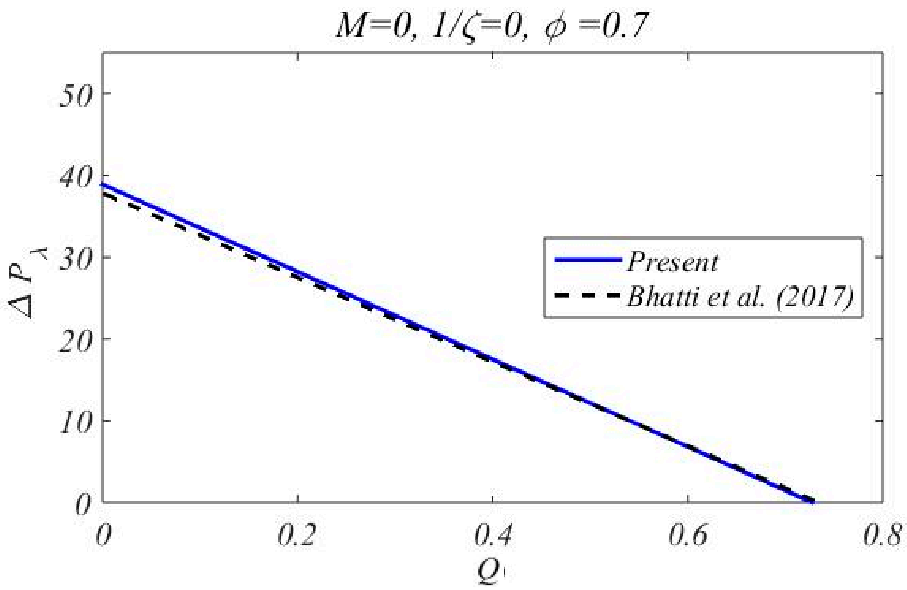


**Figure 2.** Comparison of pressure profile based on obtained results with that of Bhatti et al. (2017) [35].

Figure 3 notifies the nature of the velocity profile against the Hartmann number $M$ and the Ree–Eyring fluid parameter $\zeta$. The enhancement in the strength of the applied magnetic field dominates the electromagnetic forces in comparison to the viscous forces, which regard the motion of the flow. Therefore, the successive decrement in the magnitude of axial velocity in the center of the channel is addressed by incrementing the value of the magnetic parameter $M$, whereas one can see the counter behavior of the fluid's velocity near the boundary. The velocity variation against the Ree–Eyring fluid parameter $\zeta$ is entirely opposite on the other hand. The pressure rise per wavelength $\Delta p_\lambda$ against the time mean flow for alternating values of $M$ and $\zeta$ are respectively shown in Figure 4a,b. The increasing outcomes of pressure in the retrograde pumping zone are obvious with the elevation in the Hartmann number $M$ and Ree–Eyring parameter $\zeta$. This suggests that both these parameters have imposed a negative impact on the considered flow. Meanwhile, contrary behavior is recorded in a region called co-pumping against both parameters. The profiles of temperature dispersion as a function of the transverse coordinate $y$ are plotted in Figure 5 against several parameters such as the magnetic parameter $M$, Ree–Eyring parameter $\zeta$, and Brinkmann number $B_r$. Rising values of $M$ amply reduce the temperature profiles in the whole cross-section unless $y$ exceeding 1.3, and then the behavior is reversed. The temperature after this value rises with the rise in $M$ adjacent to the channel boundaries but is less significant. After this, the escalated values of $\zeta$ and $B_r$, as can be seen, visibly impart the increasing effect on the temperature distribution. the Brinkmann number is the ration of the heat produced to the viscous dissipation to the heat transported by molecular conduction. So, the enhancement in the Brinkmann number increases the heat inflow to the system, which consequently raises the temperature of the fluid flow. Larger values of the Brinkmann number $B_r$ are responsible for enhancing viscous heat generation in the flow, which eventually results in a rising temperature. Henceforth, the results are recorded for entropy generation associated with involved physical parameters in our discussion. Figure 6 delineates entropy generation in view of the Hartmann number $M$ and Ree–Eyring parameter $\zeta$. It is obvious that the enhanced values of $M$ initially upsurge the entropy profiles, which almost dominate across the region except near the peristaltic walls. $\zeta$ intensifies entropy generation, which is vivid, but with the increase in $y$, the profiles, seem to be much closer. In Figure 7, the entropy distribution is visualized in view of the Brinkmann number $B_r$ and temperature difference parameter $\Lambda$. It is evident from the graphs that by enlarging either $B_r$ or $\Lambda$, a noteworthy increase in entropy is manifested. The rise in internal energy of the fluid takes place with the strengthening of the fluid's viscous forces, and, in turn, dissipation occurs along with, consequently, the entropy. Further, the mechanism that notably discloses the formation of moving masses (bolus) in peristaltic transmission, which are grasped by virtue of streamlines in the shape of round trajectories, is named trapping. The contours of the streamlines influenced by various pertinent parameters are explained through plots 8–10. Figure 8 is concerned with the contouring of streamlines in view of the variable values of the magnetic parameter $M$. It is clear that both the number and size of the bolus were reduced by the increasing Lorentz force. In Figure 9, the Ree–Eyring fluid $\zeta$ parameter, in contrast with the previous case, conveys the increasing effects on the number and size of the bolus. With enlargement in the values of $\zeta$, and a rapid and visible increase in the boluses, thus, has been judged. Figure 10 is plotted to display the variation in streamlines caused by the alternating amplitude ratio $\phi$. The depicted results are again the same as we had narrated for $\zeta$, except that much more boluses emerged. This supports that $\phi$ augments the flow rate and also happens to be more influential to create the bolus.

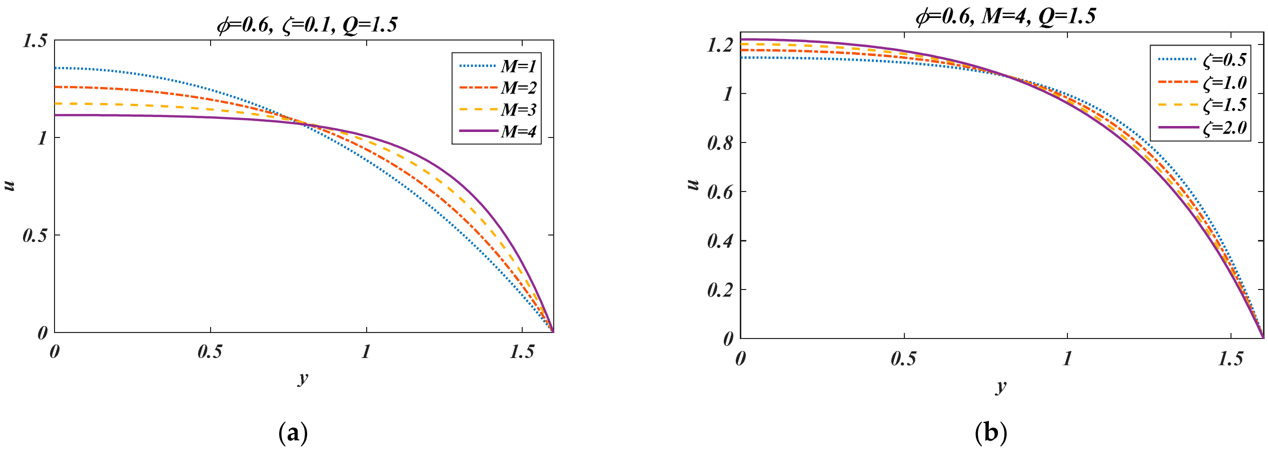


**Figure 3.** Variation in velocity for different values of (**a**) Hartmann number $M$ and (**b**) Casson parameter $\zeta$.

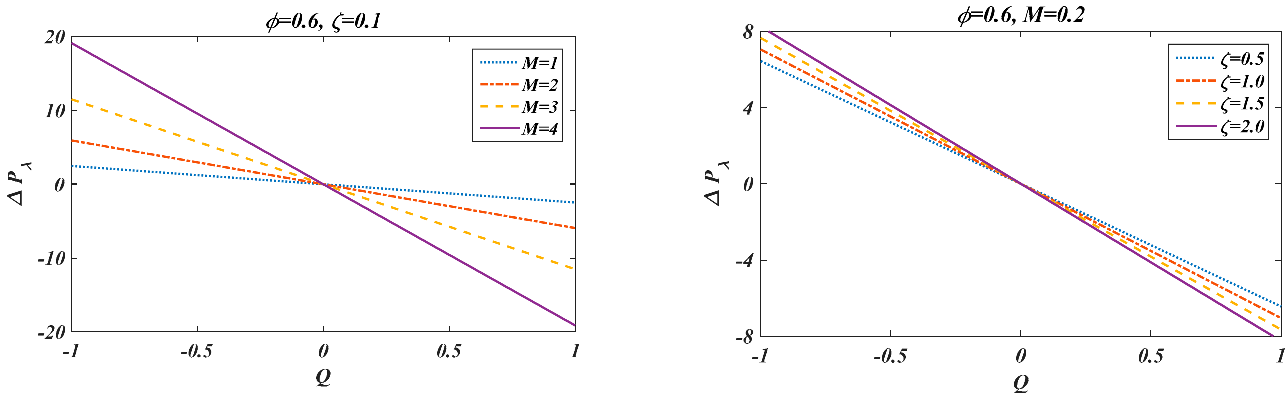


(a) (b)

**Figure 4.** Pressure rises per wavelength for different values of (**a**) Hartmann number $M$ and (**b**) Casson parameter $\zeta$.

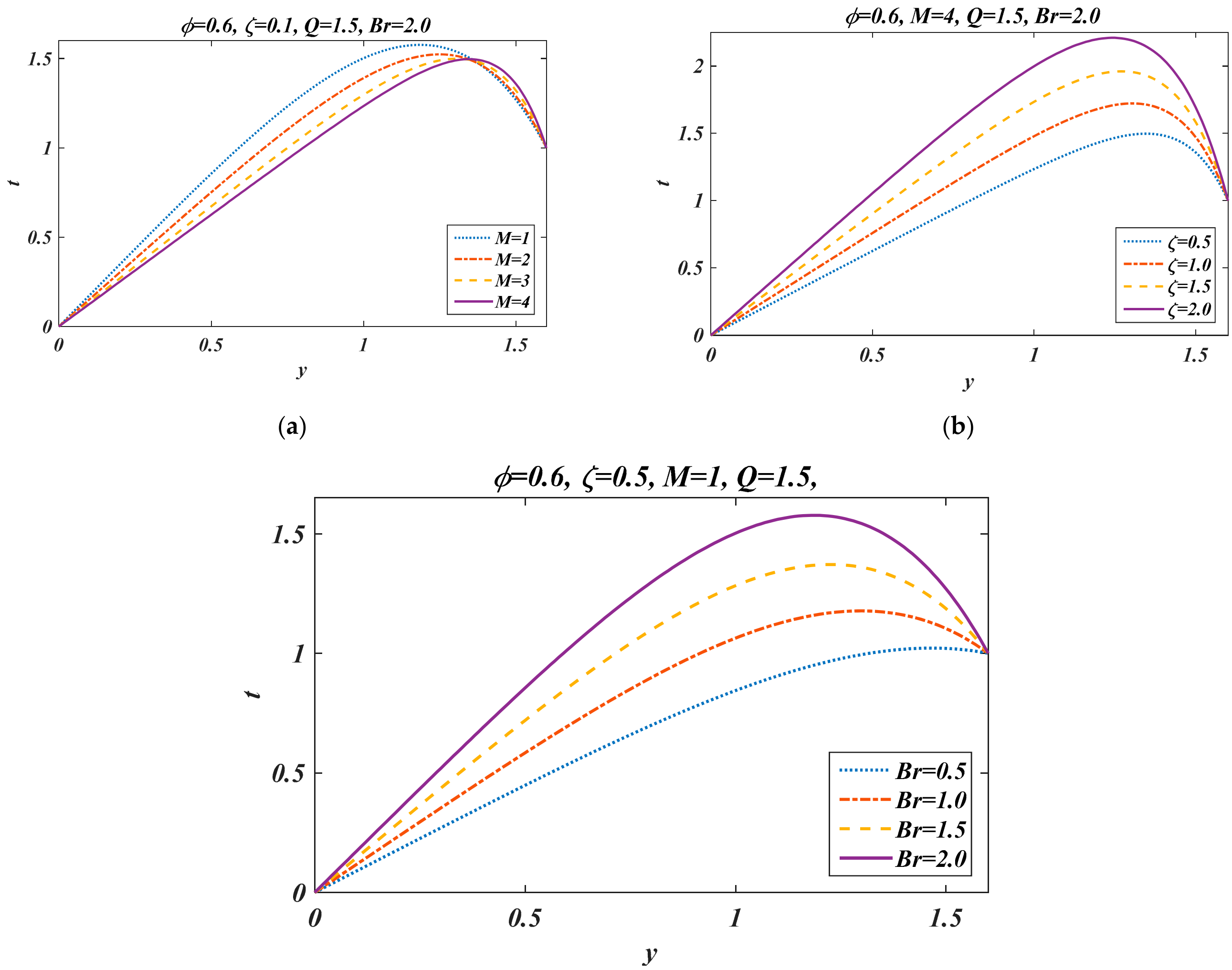


(c)

**Figure 5.** (**a**) Temperature distribution for different values of Hartmann number $M$ (**b**) Different values of Casson parameter $\zeta$ and (**c**) Different values of Brinkmann number $B_r$.

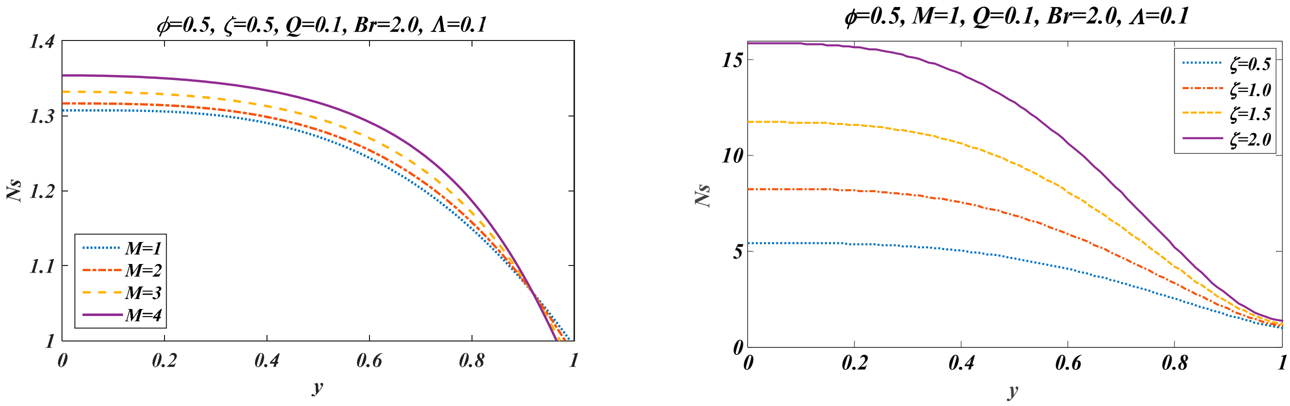


(**a**) (**b**)

**Figure 6.** Entropy generation for different values of (**a**) Hartmann number $M$ and (**b**) Casson parameter $\zeta$.

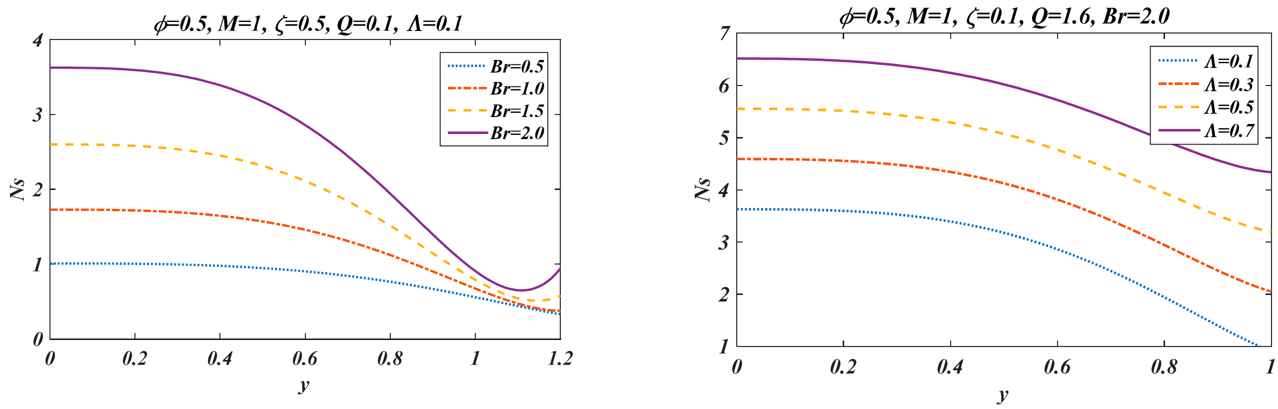


(**a**) (**b**)

**Figure 7.** Entropy generation for different values of (**a**) Brinkmann umber $B_r$ and (**b**) different values of temperature difference paramter $\Lambda$.

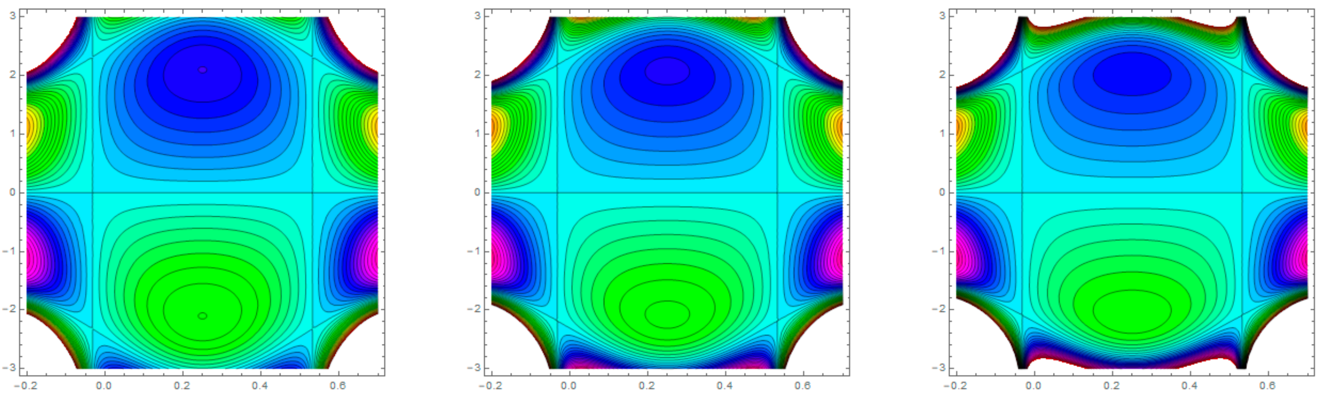

(**a**) (**b**) (**c**)

**Figure 8.** Streamlines for different values of $M$ with fixed values of $\phi = 0.5,\ \zeta = 0.5, \overline{Q} = 0.1$ (**a**) $M = 2$, (**b**) $M = 3$, and (**c**) $M = 4$.

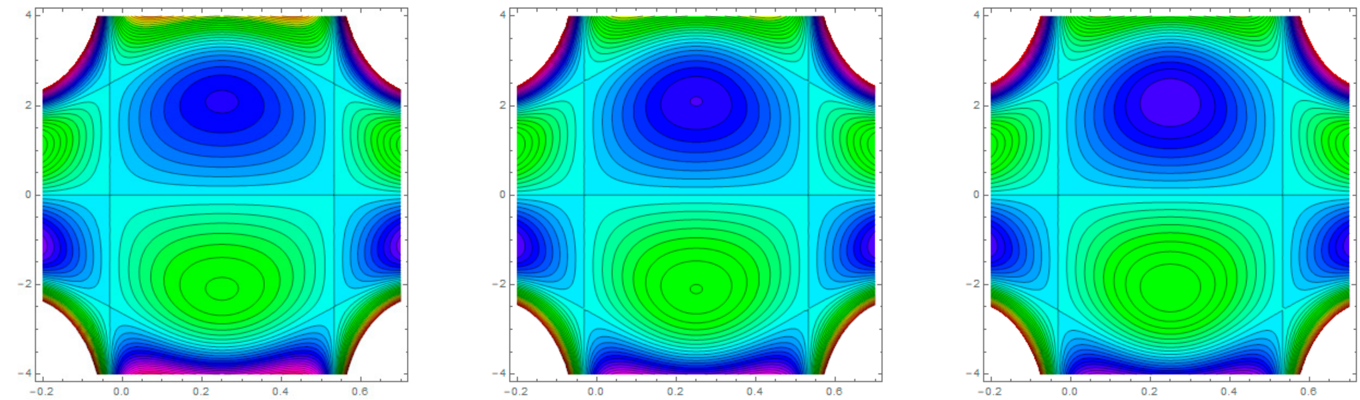


(**a**) (**b**) (**c**)

**Figure 9.** Streamlines for different values of $\zeta$ with fixed values of $M = 1,\ \phi = 0.5, \overline{Q} = 0.1$ (**a**) $\zeta = 0.5$, (**b**) $\zeta = 2.0$, and (**c**) $\zeta = 5.0$.

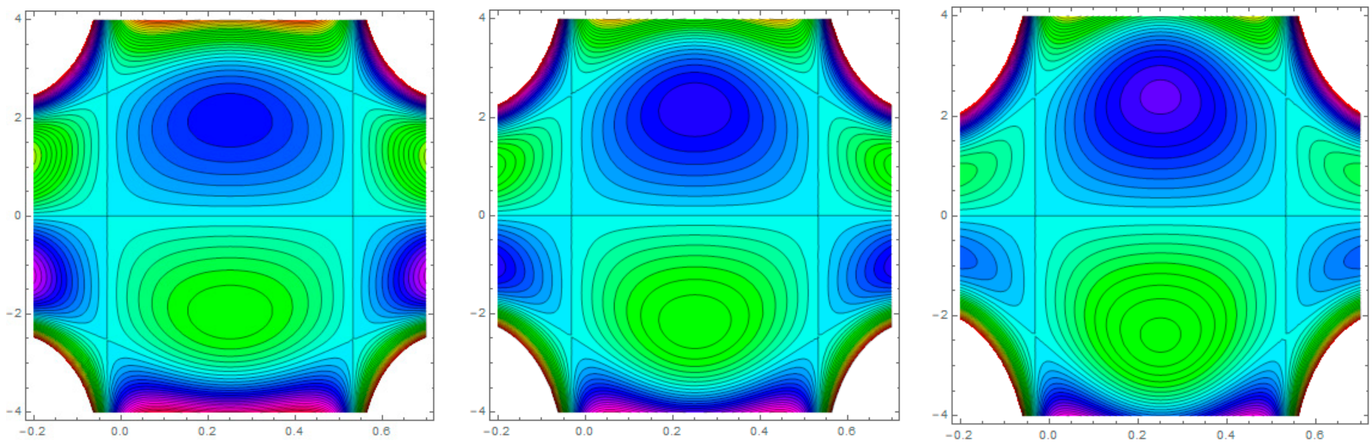


(**a**) (**b**) (**c**)

**Figure 10.** Streamlines for different values of $\phi$ with fixed values of $M = 1,\ \zeta = 0.5, \overline{Q} = 0.1$ (**a**) $\phi = 0.4$, (**b**) $\phi = 0.6$, and (**c**) $\phi = 0.8$.

## 6. Closing Remarks

The impacts of MHD on the peristaltic flow of the Ree–Eyring fluid have been inspected in the current analysis, and entropy generation was also taken into account. The modeled equations displaying the peristaltic motion for the Ree–Eyring fluid in a non-uniform symmetric channel in attendance of a uniformly applied magnetic field have been simplified using the implications of lubrication theory. The resulting ordinary differential equations have been sorted out by employing the exact method and are presented as the closed-form solution. The crucial findings of the current investigation are significantly shown:

- The velocity profile shows symmetric and the opposite behavior with the enhancement in the Hartmann number and Ree–Eyring parameter.
- When the Hartmann number is allowed to elevate, it has been investigated that a pressure rise causes an upsurge in the retrograde region but displays the reverse action in the co-pumping region. Almost the same trend is manifested in the case of the Ree–Eyring parameter.
- The amplification in the case of entropy generation is analogous to variations in all parameters, while the Hartmann number shows a slight deviation in the vicinity of boundaries.

- Temperature dispersion arguments with the rising values of the Brinkmann number and Ree–Eyring parameter.
- With elevating values, both the Hartmann number and Ree–Eyring parameter convey an opposite impact on the formation of streamlined trajectories.

**Author Contributions:** K.A. provided the formal analysis of the flow situation and modelled the flow phenomenon, B.A. supervised and dimensionalized the governing equations and performed the simulation followed by plotting the graphs, A.U.K.N. provided the discussion on the results evaluated by B.A. and the writing—original draft preparation, and conclusion was undertaken by M.A. All authors have read and agreed to the published version of the manuscript.

**Funding:** This work was supported by the Deanship of Scientific Research, Vice Presidency for Graduate Studies and Scientific Research, King Faisal University, Saudi Arabia [Grant No. 2469].

**Data Availability Statement:** No new data were created, or where data is unavailable due to privacy or ethical restrictions.

**Conflicts of Interest:** The authors declare no conflict of interest.

## References

1. Johnson, K.L. Non-Newtonian Effects in Elastohydrodynamic Lubrication. In *Tribology Series*; Elsevier: Amsterdam, The Netherlands, 1993; Volume 25, pp. 15–26.
2. Nouri, J.M.; Umur, H.; Whitelaw, J.H. Flow of Newtonian and non-Newtonian fluids in concentric and eccentric annuli. *J. Fluid Mech.* **1993**, *253*, 617–641. [CrossRef]
3. Chhabra, R.P.; Richardson, J.F. *Non-Newtonian Flow and Applied Rheology: Engineering Applications*; Butterworth-Heinemann: Boston, MA, USA, 2011.
4. Molla, M.; Yao, L. Mixed convection of non-Newtonian fluids along a heated vertical flat plate. *Int. J. Heat Mass Transf.* **2009**, *52*, 3266–3271. [CrossRef]
5. Sochi, T. Flow of non-Newtonian fluids in porous media. *J. Polym. Sci. Part B Polym. Phys.* **2010**, *48*, 2437–2767. [CrossRef]
6. Ryltseva, K.; Borzenko, E.; Shrager, G. Non-Newtonian fluid flow through a sudden pipe contraction under non-isothermal conditions. *J. Non Newton. Fluid Mech.* **2020**, *286*, 104445. [CrossRef]
7. Latham, T.W. Fluid Motions in a Peristaltic Pump. Ph.D. Thesis, Massachusetts Institute of Technology, Cambridge, MA, USA, 1966.
8. Nadeem, S.; Akram, S. Peristaltic flow of a Williamson fluid in an asymmetric channel. *Int. J. Nonlinear Sci. Numer. Simul.* **2010**, *15*, 1705–1716. [CrossRef]
9. Akram, S.; Sohail, N.; Anwar, H. Partial slip consequences on peristaltic transport of Williamson fluid in an asymmetric channel. *Walailak J. Sci. Technol. (WJST)* **2015**, *12*, 885–908.
10. Akram, S.; Sohail, N. Analytical analysis of peristaltic flow of a 6 constant Jeffreys model of fluid in an inclined planar channel. *Walailak J. Sci. Technol. (WJST)* **2014**, *11*, 129–148.
11. Pandey, S.K.; Tripathi, D. Peristaltic transport of a Casson fluid in a finite channel: Application to flows of concentrated fluids in oesophagus. *Int. J. Biomath.* **2010**, *3*, 453–472. [CrossRef]
12. Ellahi, R.; Bhatti, M.M.; Vafai, K. Effects of heat and mass transfer on peristaltic flow in a non-uniform rectangular duct. *Int. J. Heat Mass Transf.* **2014**, *71*, 706–719. [CrossRef]
13. Riaz, A.; Nadeem, S.; Ellahi, R.; Zeeshan, A. Exact Solution for Peristaltic Flow of Jeffrey Fluid Model in a Three Dimensional Rectangular Duct having Slip at the Walls. *Appl. Bionics Biomech.* **2014**, *11*, 81–90. [CrossRef]
14. Abbas, M.A.; Bai, Y.; Bhatti, M.M.; Rashidi, M.M. Three dimensional peristaltic flow of hyperbolic tangent fluid in non-uniform channel having flexible walls. *Alex. Eng. J.* **2016**, *55*, 653–662. [CrossRef]
15. Imran, M.; Shaheen, A.; Sherif, E.-S.M.; Rahimi-Gorji, M.; Seikh, A.H. Analysis of peristaltic flow of Jeffrey six constant nano fluid in a vertical non-uniform tube. *Chin. J. Phys.* **2020**, *66*, 60–73. [CrossRef]
16. Basha, H.; Sivaraj, R. Entropy generation of peristaltic Eyring–Powell nanofluid flow in a vertical divergent channel for biomedical applications. *Proc. Inst. Mech. Eng. Part E J. Process. Mech. Eng.* **2021**, *235*, 1575–1586. [CrossRef]
17. Ebaid, A. A new numerical solution for the MHD peristaltic flow of a bio-fluid with variable viscosity in a circular cylindrical tube via Adomian decomposition method. *Phys. Lett. A* **2008**, *372*, 5321–5328. [CrossRef]
18. Akbar, N.S. Influence of magnetic field on peristaltic flow of a Casson fluid in an asymmetric channel: Application in crude oil refinement. *J. Magn. Magn. Mater.* **2015**, *378*, 463–468. [CrossRef]
19. Sinha, A.; Shit, G.C.; Ranjit, N.K. Peristaltic transport of MHD flow and heat transfer in an asymmetric channel: Effects of variable viscosity, velocity-slip and temperature jump. *Alex. Eng. J.* **2015**, *54*, 691–704. [CrossRef]
20. Bhatti, M.M.; Ellahi, R.; Zeeshan, A. Study of variable magnetic field on the peristaltic flow of Jeffrey fluid in a non-uniform rectangular duct having compliant walls. *J. Mol. Liq.* **2016**, *222*, 101–108. [CrossRef]

21. Abbas, M.A.; Bai, Y.Q.; Rashidi, M.M.; Bhatti, M.M. Application of Drug Delivery in Magnetohydrodynamics Peristaltic Blood Flow of Nanofluid in a Non-Uniform Channel. *J. Mech. Med. Biol.* **2016**, *16*, 1650052. [CrossRef]
22. Abd-Alla, A.M.; Thabet, E.N.; Bayones, F.S. Numerical solution for MHD peristaltic transport in an inclined nanofluid symmetric channel with porous medium. *Sci. Rep.* **2022**, *12*, 3348. [CrossRef]
23. Bejan, A. A Study of Entropy Generation in Fundamental Convective Heat Transfer. *J. Heat Transf.* **1979**, *101*, 718–725. [CrossRef]
24. Akbar, N.S. Entropy Generation Analysis for a CNT Suspension Nanofluid in Plumb Ducts with Peristalsis. *Entropy* **2015**, *17*, 1411–1424. [CrossRef]
25. Rashidi, M.M.; Bhatti, M.M.; Abbas, M.A.; Ali, M.E.-S. Entropy Generation on MHD Blood Flow of Nanofluid Due to Peristaltic Waves. *Entropy* **2016**, *18*, 117. [CrossRef]
26. Asha, S.; Deepa, C. Entropy generation for peristaltic blood flow of a magneto-micropolar fluid with thermal radiation in a tapered asymmetric channel. *Results Eng.* **2019**, *3*, 100024. [CrossRef]
27. Bibi, A.; Xu, H. Entropy Generation Analysis of Peristaltic Flow and Heat Transfer of a Jeffery Nanofluid in a Horizontal Channel under Magnetic Environment. *Math. Probl. Eng.* **2019**, *2019*, 1–13. [CrossRef]
28. Bhatti, M.M.; Abbas, M.A.; Rashidi, M.M. Combine effects of Magnetohydrodynamics (MHD) and partial slip on peristaltic Blood flow of Ree–Eyring fluid with wall properties. *Eng. Sci. Technol. Int. J.* **2016**, *19*, 1497–1502. [CrossRef]
29. Hayat, T.; Zahir, H.; Alsaedi, A.; Ahmad, B. Heat transfer analysis on peristaltic transport of Ree-Eyring fluid in rotating frame. *Chin. J. Phys.* **2017**, *55*, 1894–1907. [CrossRef]
30. Ijaz, N.; Zeeshan, A.; Bhatti, M. Peristaltic propulsion of particulate non-Newtonian Ree-Eyring fluid in a duct through constant magnetic field. *Alex. Eng. J.* **2018**, *57*, 1055–1060. [CrossRef]
31. Hayat, T.; Akram, J.; Alsaedi, A.; Zahir, H. Endoscopy and homogeneous-heterogeneous reactions in MHD radiative peristaltic activity of Ree-Eyring fluid. *Results Phys.* **2018**, *8*, 481–488. [CrossRef]
32. Tanveer, A.; Malik, M. Slip and porosity effects on peristalsis of MHD Ree-Eyring nanofluid in curved geometry. *Ain Shams Eng. J.* **2021**, *12*, 955–968. [CrossRef]
33. Rajashekhar, C.; Mebarek-Oudina, F.; Vaidya, H.; Prasad, K.V.; Manjunatha, G.; Balachandra, H. Mass and heat transport impact on the peristaltic flow of a Ree–Eyring liquid through variable properties for hemodynamic flow. *Heat Transf.* **2021**, *50*, 5106–5122. [CrossRef]
34. Balachandra, H.; Rajashekhar, C.; Mebarek-Oudina, F.; Manjunatha, G.; Vaidya, H.; Prasad, K.V. Slip Effects on a Ree-Eyring Liquid Peristaltic Flow Towards an Inclined Channel and Variable Liquid Properties. *J. Nanofluids* **2021**, *10*, 246–258. [CrossRef]
35. Bhatti, M.M.; Abbas, M.A.; Rashidi, M.M. Entropy generation for peristaltic blood flow with Casson model and consideration of magnetohydrodynamics effects. *Walailak J. Sci. Technol. (WJST)* **2017**, *14*, 451–461.